Available online at www.sciencedirect.com
ScienceDirect
Earth and Planetary Science Letters 260 (2007) 56–71
EPSL
www.elsevier.com/locate/epsl

Magnetic anomaly map of the world: merging satellite, airborne, marine and ground-based magnetic data sets

Kumar Hemant [a,b,*], Erwan Thébault [c,d], Mioara Mandea [c], Dhananjay Ravat [e], Stefan Maus [f]

[a] School of Earth and Environment, University of Leeds, Leeds, UK
[b] Goddard Space Flight Center, NASA, Greenbelt, USA
[c] GeoForschungsZentrum, Potsdam, Germany
[d] Institut de Physique du Globe de Paris, Jussieu, France
[e] Southern Illinois University C'dale, Carbondale, IL, USA
[f] National Geophysical Data Center, NOAA, Boulder, CO, USA

Received 1 September 2006; received in revised form 9 May 2007; accepted 10 May 2007
Available online 31 May 2007
Editor: T. Spohn

Abstract

We report here a simple but practical method to combine systematically the magnetic surveys of disparate specifications from marine, ground, aeromagnetic and satellite platforms that aims to be helpful in the framework of the world digital magnetic anomaly map project. Because the satellite coverage and data quality is more uniform than near-surface surveys, it is adopted as the base map for wavelengths larger than 400 km and up to spherical harmonic degree inclusive of 16 (~2500 km). After checking that satellite models and large aeromagnetic wavelengths are not consistent, we filter out wavelengths longer than 400 km in aeromagnetic compilations. Existing regional grids and, when available, individual surveys, are merged to give a more uniform spatial variation of the magnetic anomalies. The effects of merging the grids are examined by plotting profiles and difference maps of the overlapping regions. A preliminary global map is obtained after combining the magnetic anomaly map with the downward continued CHAMP satellite derived magnetic anomaly map. Forthcoming availability of new datasets, as well as improvements in the procedure, will help to produce increasingly reliable maps.
© 2007 Elsevier B.V. All rights reserved.

Keywords: world digital magnetic anomaly map; LEEDS-WDMAM candidate model; aeromagnetic and marine compilation

1. Introduction

Magnetic surveys, both airborne and marine, have played a key role in unraveling the structure and dynamics of the Earth's surface (Vine, 1966; Pilkington and Todoeschuck, 1993; Blakely et al., 2000). There are a number of important geologic problems which are difficult to solve using the existing separate grids, mainly because repeated rifting, movement, and assembly of the landmasses over billions of years have made once adjacent geologic provinces move to completely different parts of the world (Reeves and de Wit, 2000). A consistent world magnetic anomaly map will aid evaluation of hypotheses of geologic origin of such regions. In addition, numerous

* Corresponding author. School of Earth and Environment, University of Leeds, Leeds, UK.
E-mail address: hemant@earth.leeds.ac.uk (K. Hemant).

0012-821X/$ - see front matter © 2007 Elsevier B.V. All rights reserved.
doi:10.1016/j.epsl.2007.05.040

scientific problems can be addressed by magnetic anomaly data for understanding the variable structure, temperature, and rheology of the lithosphere (Blakely and Simpson, 1986; Griscom and Jachens, 1989; Behrendt et al., 1998). These studies require consistently prepared data sets over thousands of kilometers of distance.

Toward this end, efforts are being made to compile a world magnetic anomaly map by combining ground-based, airborne and marine magnetic data, under the auspices of the World Digital Magnetic Anomaly Map (WDMAM) task force of IAGA's working group V-MOD. IAGA's charge to the WDMAM committee is general: it is to produce a compiled magnetic anomaly map consisting of all possible wavelengths that would be useful for geological and tectonic mapping of the Earth's crust. We propose here a candidate model for the WDMAM project and also outline and illustrate the difficulties one has to face for obtaining a self-consistent global map. We thus describe in detail the different steps leading to the final map. In this paper, we adopt a basic approach that consists of using near-surface magnetic data for the short wavelength part of the map and a satellite derived global magnetic anomaly map for the long wavelength anomaly coverage. We therefore take advantage of the strengths of each data set while bypassing its limitations. For example, wavelengths smaller than 400 km are naturally attenuated in the present satellite data due to their high observation altitude (~400 km), whereas the shorter wavelength part of the anomaly spectrum are reliably mapped by near-surface compilations. In the same vein, magnetic compilations result from a patchwork of regional surveys, carried out at different epochs and altitudes, and with different instrumentation. Thus, merging aeromagnetic data of varying quality, which were reduced using different procedures and core field models, causes significant differences and leveling errors between separately collected/processed adjacent magnetic surveys (Ravat et al., 2003). As a result, the near-surface compilations do not readily merge with one another and long wavelength components of the lithospheric field are not retained adequately.

Continental scale compilations exist over North America (Bankey et al., 2002) and Antarctica (Kim et al., 2004), but no global compilation has been attempted until now because the challenge of handling the number of grids and their specification differences has been overwhelming. With persistent efforts during the last few years, a large number of aeromagnetic and marine data sets are now freely accessible. In addition, new high resolution magnetic field models based on the observations of the three most recent satellite missions Ørsted, SAC-C and CHAMP enable us to gradually close the spectral gap between satellite and near-surface data. Using the available aeromagnetic and satellite magnetic anomaly grids, five candidate models have now been produced by teams at the Geological Survey of Finland (GTK), GSFC–NASA, GeoForschungsZentrum (Hamoudi et al., in press), NGDC (Maus et al., in press) and University of Leeds (http://projects.gtk.fi/WDMAM/project/). The model (LEEDS-WDMAM), which is proposed here, is the one produced by the University of Leeds group.

One of the necessities of the world magnetic anomaly map is that the process of making the map will have to be undertaken repeatedly with the availability of additional and/or better quality data. In addition, the forthcoming *Swarm* mission of the European Space Agency (ESA, 2004), will considerably improve the situation and provide new highly accurate and high resolution satellite measurements. Thus, we need simple, but effective methods to reliably synthesize a map which accurately represents the world's magnetic anomalies. After a review of the different available compilations and their specifications, we describe our scheme to remove the large wavelengths by filtering and present a simple way to merge the grids and trackline data. Complementary large wavelengths (>400 km wavelength) are subsequently added using a downward continued lithospheric magnetic field model at the marine, ground or aeromagnetic level. We finally discuss different techniques and improvements of differing complexity that could help to further improve the accuracy of the World Digital Magnetic Anomaly Map.

2. Data sets and preliminary processing

The available coverage of airborne, marine and ground-based magnetic data sets is shown in Fig. 1. The figure shows an almost complete coverage over both hemispheres. Data gaps can still be seen over parts of Saudi Arabia and India, much of Africa and South America. Large sets of NGDC marine data including the data from Project Magnet (Smith and Ravat, 2005, 2006) are now processed and available for the WDMAM project. The available metadata information from the compilations shows the coverage to be in various projections and datums depending on their geographical representation on the globe. The details are shown in Table 1. The sources of these compilations are referenced in the last column.

As magnetic compilations are available in various formats and projections, before applying any filtering or merging procedures, all grids (digital magnetic anomaly maps or compilations are termed grids hereafter) are

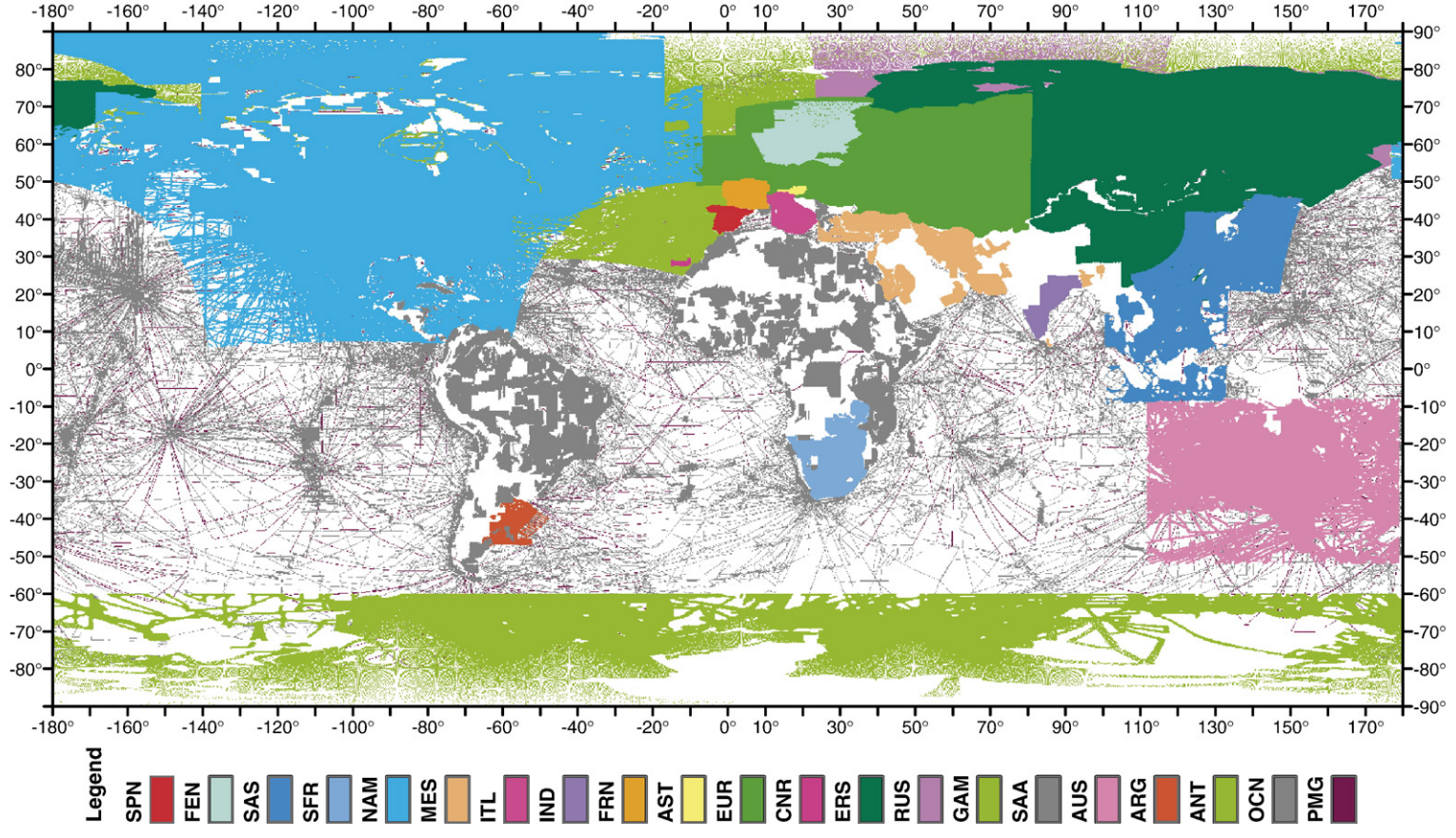

Fig. 1. Global coverage of available airborne, marine and ground-based magnetic data sets. The details of these data sets are mentioned in Table 1.

Table 1
Summary of the metadata information of available airborne, marine and ground-based magnetic data sets

Region	Grid resolution	Coordinate system	Reference
Europe (EUR)	5.0 km	Lambert Conic Conformal	http://www.bgr.bund.de/, Wonik et al. (2001)
North America (NAM)	1.0 km	NAD27	NAMAG, http://pubs.usgs.gov/sm/map_map/ Bankey et al. 2002)
Arctic and North Atlantic (GAM)	5.0 km	Geographic	http://gsc.nrcan.gc.ca/, Verhoef et al. (1996)
Middle East and India (in part) (MES)	1.0 km	Geographic	AAIME, http://home.casema.nl/errenwijlens/itc/aaime/ Reeves (2003)
Australia (AUS)	1.0 km	Geographic	Geoscience Australia, http://www.ga.gov.au/ Petkovic and Milligan (2002)
Eurasia (ERS)	2.0 km	Geographic	GSC, http://gsc.nrcan.gc.ca/
Russia (RUS)	5.0 km	VSEGEI 2006	VSEGEI, http://www.vsegei.ru/WAY/247038/locale/EN/
Antarctica (ANT)	5.0 km	Geographic	ADMAP, http://www.geology.ohio-state.edu/geophys/admap/ Golynsky et al. (2002)
South East Asia (SAS)	2.0 km	Geographic	CCOP, http://www.ccop.or.th Ishihara and Kisimoto (1996)
France (FRN)	7.0 km	Lambert II etendu	Le Mouel (1969)
Italy (ITL)	5.0 km	Geographic	Chiappini, C., *Annali di Geofisica, Vol 45*, *5*, 2000
Fennoscandia (FEN)	5.0 km	WGS84	GTK, http://www.gtk.fi
Spain (SPN)	2.5–10 km	UTM 33N	Socias, I., *Earth Planet Sci Lett.*, *105*, *55–64*, 1991
Canary Island (CNR)	5.0 km	UTM 28N	IGN, *Publi. Tec.*, *No 35*, *Madrid*, 1996
Austria (AST)	5.0 km	GK, M31	GSA, http://www.geologie.ac.at
South Africa (SFR)	5.0 km	Geographic	SADC, http://www.sadc.fi
Africa and South America (SAA)	15 min	Geographic	GETECH, http://www.getech.com
Argentina inland (ARG)	5.0 km	N/A	SEGEMAR, http://www.segemar/gov.ar
Argentina margin (ARG)	5.0 km	Geographic	Ghidella, DNA, http://www.dna.gov.ar
India (IND)	5.0 km	Geographic	GSI, http://www.gsi.gov.in/
Project Magnet (PMG)	profiles	Geographic	NGDC, http://www.ngdc.noaa.gov/seg/geomag/proj_mag.shtml
Marine data, NGDC (OCN)	profiles	Geographic	NGDC, http://www.ngdc.noaa.gov/mgg/geodas/trackline.html
MF5		Geographic	http://www.gfz-potsdam.de/pb2/pb23/index.html

Some resolutions are given in arc minute.

transformed from their local reference system to a common representation on the global reference ellipsoid, WGS84 using conversion formulas (Snyder, 1987). Marine data were reprocessed to produce grids at mean sea level (Smith and Ravat, 2006).

The continental scale aeromagnetic compilations shown in Table 1 are produced after stitching together many regional anomaly grids. These regional surveys were flown at different times and, hence, use different main field models to reduce the observed data. The patch work grids are prone to offsets, and mismatch in anomaly shapes and differences are clearly noticeable across overlapping regions. They have the potential of introducing fictitious anomalies (Whaler, 1994; Ravat et al., 2002). The lack of absolute reference makes it difficult to recover this long wavelength information. Despite their decimation on a regular grid, the final resolution may not be uniform and only a spectral analysis such as wavelet techniques could help locating precisely the regions of varying resolution. These inconsistencies were also highlighted in earlier versions of the aeromagnetic map of the U.S. (Zietz, 1982). Further, the main field models used to reduce these regional surveys are mostly unknown as each individual compilation panel was usually reduced using a local polynomial. This lack of information prevents us from further correcting the grids for a more homogeneous core field model. We decided to avoid the further integration of inconsistent long wavelengths and artificial discontinuities between adjacent compilations by simply filtering the data. In the following, according to the WDMAM recommendations, the grids are resampled to 0.05° (11 km wavelength at the Equator).

3. Continuity of the grids

A typical global magnetic anomaly map can be derived by stitching together all the available grids. The available data sets are: Australia (AUS), North America (NAM), Middle East (MES), South Asia (SAS), Austria (AST), Italy (ITL), Spain (SPN), Fennoscandinavia (FEN), France (FRN), Eurasia (ERS), Europe (EUR), Russia (RUS), Arctic and North Atlantic (GAM), Argentina (ARG), South Africa (SFR), Canary Island (CNR), India (IND), Antarctica (ANT), Africa and South America (SAA) , NGDC oceanic grid (OCN) and Project Magnet data (PMG). The grid acronyms shown in parentheses are frequently used in the following sections.

An example of the detailed anomaly features are compared for overlapping regions between the EUR and

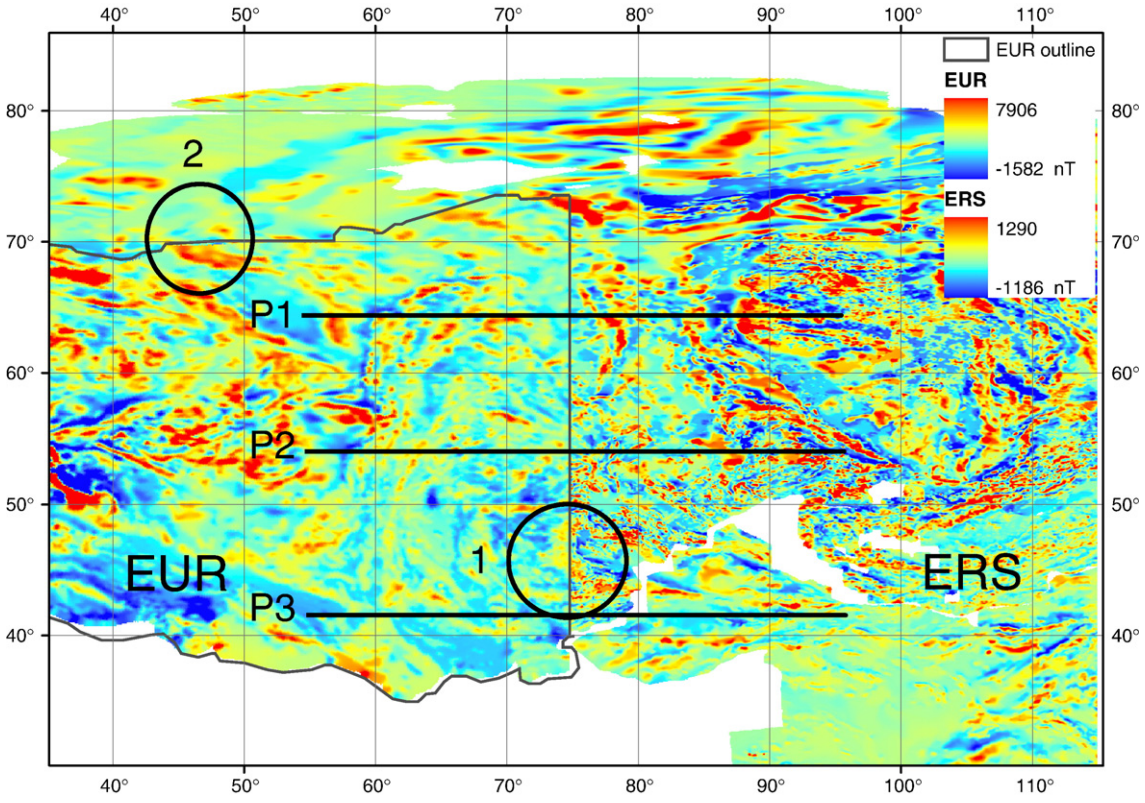

Fig. 2. The figure show detailed anomaly features between EUR and ERS grids only.

ERS grids in Fig. 2. The EUR grid shows anomalies that are smoother than the neighboring ERS grid. Two reasons may be invoked. Firstly, the EUR grid is upward continued to 3 km altitude (Wonik et al., 2001) while the ERS grid is produced by combining many disparate aeromagnetic surveys of smaller dimension without upward continuing the final grid. Secondly, spectral analysis of the EUR grid showed sudden power decay for wavelengths smaller than 30 km and it seems that the EUR grid was filtered in order to produce a homogenous resolution map. The anomaly features across the boundary of the EUR and ERS grids show partial disagreement. For instance, the anomaly feature across the regions marked as 1 in Fig. 2 appears to continue across the grid edges but the strength of the anomaly over the EUR grid appears weaker. The region marked by a circle at 2 shows a disagreement in anomaly trends across the boundary. The profiles P1, P2 and P3 shown in Fig. 3 compare the strength of total field intensities across the two grids. All profile sections show intensity variations of the ERS grid that are consistent with anomaly patterns of the EUR grid. However, within the overlapping region total field intensities marked by vertical arrows in all profile sections in Fig. 3 disagree in strength by 10–200 nT. At the grid boundary these intensities vary by 100–150 nT highlighting once again the differences in the anomaly strength across the two grids. The discrepancies shown by circles in Fig. 3 are not clearly visible in Fig. 2. Although significant disagreement between anomaly patterns of the EUR and ERS grids is not apparent in Fig. 2, the differences established through profiles in Fig. 3 indicate possible errors in the long wavelength content of the two grids; they could also be attributable to the relative difference in the anomaly strength and resolution. Such differences are also observed between the GAM and the NAM grid boundaries (not shown here). There is, however, a good agreement in the anomaly patterns across the AUS and SAS grids.

4. Merging grids

4.1. Filtering grids

To minimize differences in the anomalies between various grids, as demonstrated for the EUR and ERS grids (Section 3), we use the following procedure: A low-pass Gaussian filter with a cut-off wavelength 400 km is applied to each decimated grid in the 2-D

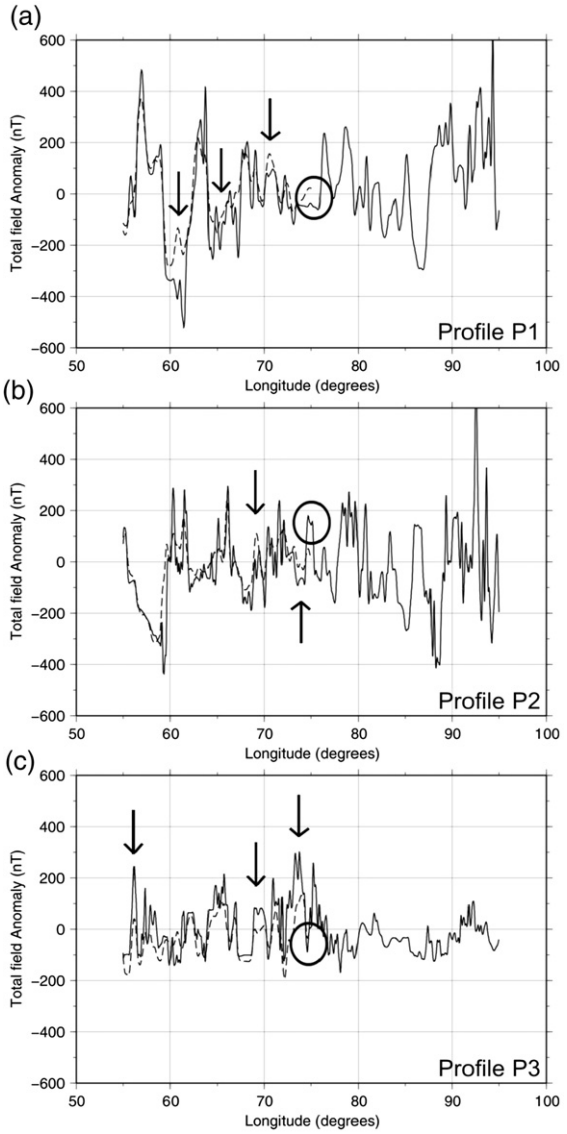

Fig. 3. Profiles sections marked in Fig. 3 along P1, P2 and P3 shown respectively in (a), (b) and (c) above. Solid line shows the total field anomaly variation for ERS grid along the profile section while the EUR grid is represented with a dashed line. The region left of (~75° E) where the dashed line terminates (grid edges) is the overlapping region between EUR and ERS grids. Differences in anomalies are highlighted by arrows within the overlapping region and by a circle at the grid edges.

space domain using the GMT software (Wessel and Smith, 2004). The cut-off frequency is set to 400 km because the longer wavelengths are later substituted by the CHAMP satellite global anomaly field model, which is robust up to spherical harmonic 100° (~400 km). The filtered output is a long wavelength (LW) grid showing anomaly features of wavelength larger than 400 km. The short wavelength (SW) grid, showing features smaller than 400 km, is obtained by subtracting the long wavelength grid from the original decimated grid. The SW and LW grids for the European compilation are shown in Fig. 4. As expected, the SW map shows much finer details of the regional geology and crustal structures. On the other hand, the LW map more strongly resembles a satellite-derived magnetic anomaly map.

4.2. Problems in the long wavelength grids based on near-surface data

In Table 2 we show a comparison of the LW components with the original datasets in order to justify the filtering procedure used here. After filtering, the long wavelength (>400 km) grids were plotted together (not shown here). LW grids showed anomaly features that resemble Fig. 4(a). To systematically analyze possible errors in the LW grids, the difference in the LW grids was computed and plotted. Fig. 5 shows variations in the difference of the amplitude of anomalies of the merged LW grids. No particular precedence order was followed here while merging grids. Table 2 shows the maximum and minimum difference between the merging grids. Table 2 and a visual inspection of Fig. 5 show that there are large differences in the LW anomalies, and often anomalies show a lack of continuity across two or more grids being merged. If the parent grids are merged without removing the erroneous LW component, the resulting product will have serious defects. The overlapping regions are demarcated by boundary lines on Fig. 5 as appropriate, in particular in the northern hemisphere where grids have large overlaps. Because it is difficult to judge which overlapping LW map is more trustworthy, and because a reliable, uniform CHAMP magnetic field map is available which can be substituted in its place, we removed the LW from the magnetic anomaly grids prior to the grid merging.

4.3. Short wavelength grids

Merging short wavelength (SW) anomalies from different grids is also non-unique where these grids differ in overlapping regions. The process is cumbersome and conducive to introducing fictitious anomalies. Merging techniques involve modifying the grids within the overlying regions and near the edges and altering the strength and pattern of anomaly features. The technique often employs a weighted average of different-order surfaces such that the two adjoining maps are seamless. In this process, anomalies are modified, or at times

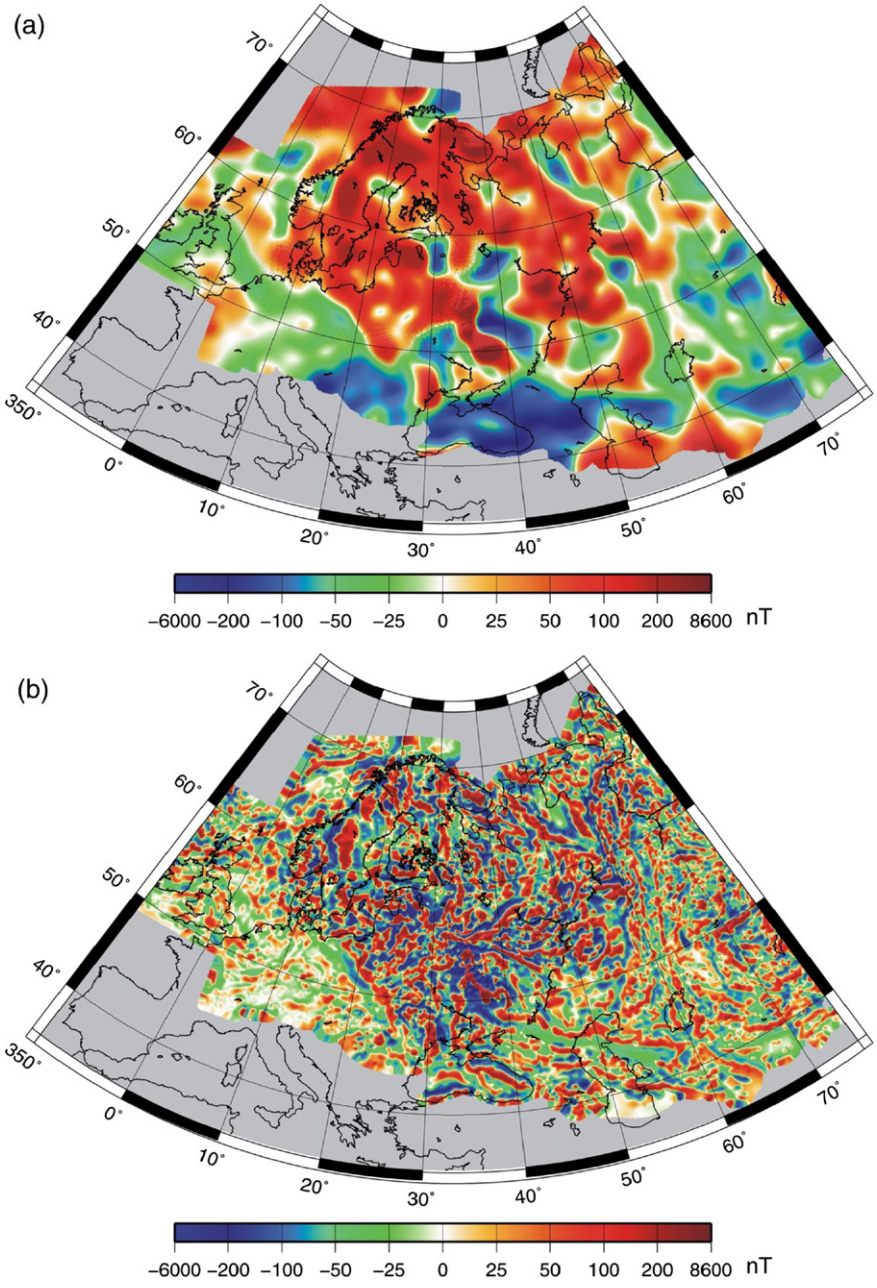

Fig. 4. Long wavelength anomalies (wavelength > 400 km) shown in (a), and short wavelength anomalies (wavelength < 400 km) shown in (b), for the European aeromagnetic compilation.

genuine crustal anomaly features are even entirely eliminated.

The merging technique used here involves an averaging procedure within the overlapping region by employing the MOSAIC tool-box of ArcInfo GIS software (http://www.esri.com/). The MOSAIC function is useful when it is desired to minimize abrupt changes along boundaries of overlapping grids. The function uses a weighted average method to calculate values of cells in the overlapping area, taking input from two or more input grids. The proximity analysis algorithm applied to determine cell values over the overlapping areas is called the Hermite Cubic and is described by the following formula (Franke, 1982):

$$H_3(s) = 1 - 3s^2 + 2s^3, \quad (1)$$

Table 2
Difference in the strength of the LW anomalies within the merging zone of the grids shown in column 1

Merging grids	Difference in strength of LW anomalies (nT)	
	Minimum (x)	Maximum (y)
EUR–AST	−116	−5
EUR–GAM	−204	449
EUR–FEN	−158	320
SPN–GAM	−10	33
GAM–RUS	−956	166
FRN–GAM	−17	43
CNR–GAM	23	145
NAM–GAM	−292	723
ERS–SAS	−78	143
ERS–RUS	−2450	199
ERS–GAM	−250	210
ERS–EUR	−730	212
SFR–SAA	−32	263
SAS–OCN	−167	378
GAM–OCN	−507	245
NAM–OCN	−445	745
AUS–OCN	−509	1345
SAA–OCN	−250	248
ANT–OCN	−205	340

where, s is the normalized distance (ranging values from 0 to 1) of the width of the overlapping area (it may be oriented horizontally or vertically). The cell values for the output C grid, being the mosaic of grids A and B on the overlapping area marked x in Fig. 6A, are calculated according to the formula (http://www.esri.com/):

$$C = A\ H + B(1 - H) \tag{2}$$

Fig. 6B shows graphically how the applied weighted average method works on the overlapping area. The ratio of weights of the overlapping grids changes within the width (s) of the x area.

The SW wavelength differences between grids vary substantially from anomaly to anomaly, and it is difficult to ascribe the order of precedence of grids on the basis of those differences. However, the quality of an individual compilation is also reflected in the LW differences. Thus, the order of precedence of the grids in this study was based on the LW differences observed between the grids (Table 2). As most of the parent grids have been prepared by stitching together many grids of varying resolution and without following a common filtering and reduction procedure, the parent grids may have errors in terms of the strength of anomaly features and their spatial extent. Thus, SW grids were merged following a precedence order based on the least difference between LW merging grid and the grid quality of the parent grid. From Table 1, AUS, MES and NAM grids have the highest spatial resolution. Thus, these grids are given the highest precedence. Both SAS and ERS are of grid resolution 2.0 km. They are next in the precedence order. Grids EUR, GAM, RUS, ANT, ITL, FEN, CNR, AST, SFR, ARG and IND are all of comparable grid resolution (5.0 km) so they follow next in the order; however, ANT, ITL, SFR, ARG and IND grids do not have a common overlapping zone with any other grids listed, so their precedence order is not important. From Table 2, the difference of the GAM and RUS grids, when compared to the ERS grid, is significantly different. Hence, GAM precedes the RUS grid. The EUR grid shows more consistent differences with GAM, FEN, and ERS, compared to the GAM grid, which shows relatively larger variations with EUR, NAM, ERS, and RUS. Hence, EUR is given higher precedence than GAM. AST can be placed before or after the EUR grid, as it overlaps only with the EUR grid. The FEN grid has no overlap with the AST grid; hence, it can follow or precede the AST grid. Interestingly, both the SPN and FRN grids show a very low difference to the GAM grid. This however does not suggest that SPN and FRN grids should precede the GAM grid. Low amplitudes of SPN–GAM and FRN–GAM (Table 2) possibly suggest that LW anomalies are poorly represented in these grids, compared to other European data sets. Hence, SPN, FRN and GAM grids were placed lower in the precedence order. The SAA grid is too sparse to contain any meaningful information for shallow crustal structures, while OCN and PMG grids comprise profile data, which need further processing to yield crustal anomaly features in the horizontal plane. In summary, the following precedence order was prepared for merging the SW grids: Australia (AUS), North America (NAM), Canary Island (CNR), South Asia (SAS), Austria (AST), Eurasia (ERS), Europe (EUR), Arctic and North Atlantic (GAM), Spain (SPN), Fennoscandia (FEN), France (FRN), Russia (RUS), Argentina (ARG), South Africa (SFR), Antarctica (ANT), Italy (ITL), India (IND), Middle East (MES), Africa and South America (SAA) , NGDC oceanic grid (OCN) and Project Magnet data (PMG). The grids were merged beginning with the highest precedence. Merging of grids was begun at the far side of the grids that are placed highest in the precedence order. Two azimuthal views of the final SW (<400 km) merged grid are shown, one for the northern hemisphere, centered over 0° longitude, and the other centered over Australia (Fig. 7).

Fig. 7 shows small-scale anomaly features of wavelength less than 400 km. Such a map is useful in mapping most near-surface geological features.

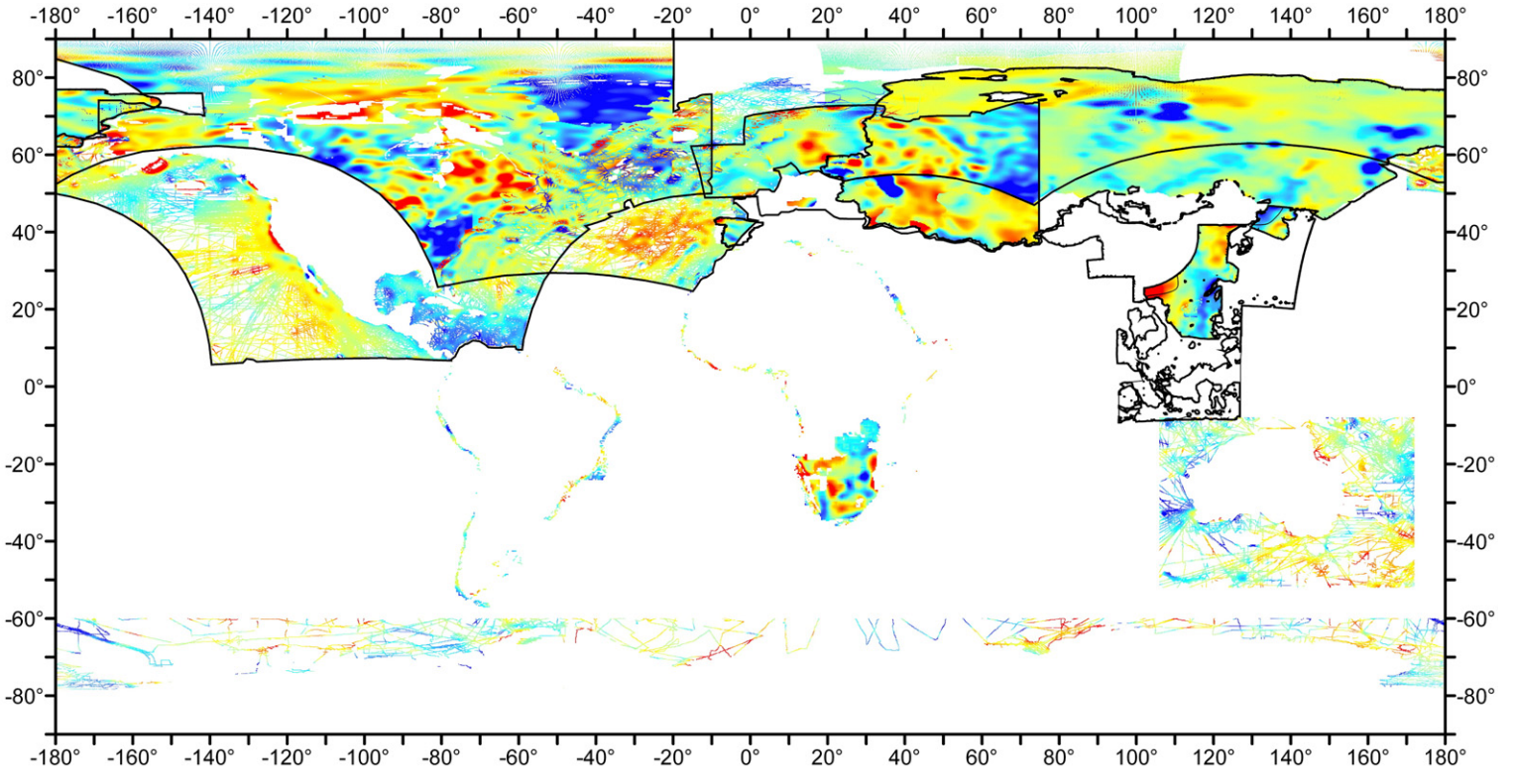

Fig. 5. Difference between Long wavelength anomalies (wavelength > 400 km) for grids shown in Fig. 1. The black line marks the grid boundaries. Not all grid boundaries are shown.

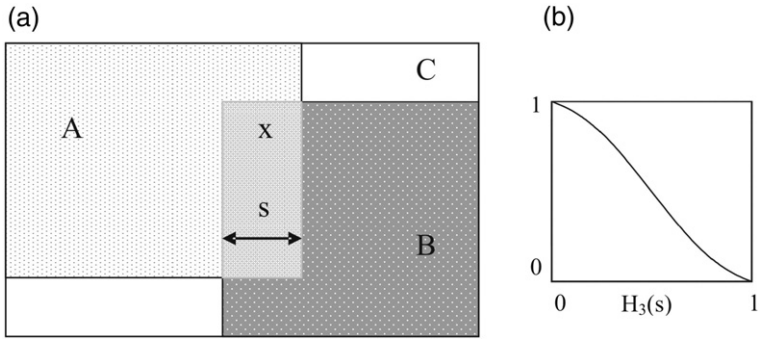

Fig. 6. (a) The diagram illustrates the merging zone x for two merging grids A and B. C is the output grid and s is the normalized distance (ranging values from 0 to 1) of the width of the overlapping area. (b) The diagram shows graphically how the applied weighted average method works on the overlapping area. The ratio of weights of the overlapping grids changes within the width (s) of the x area. The figures have been reproduced from www.esri.com/.

Numerically, the accuracy and reliability of the merged product is assessed by investigating the effect of merging on the continuity of anomaly patterns across two or more grids and the effects on the anomaly shapes and strengths within and near the grid boundary. This can be verified from profile Sections 1 and 2 shown in Fig. 8a–c. Profiles compare the anomalies between the EUR and ERS grids. Following our precedence order, the ERS grid precedes EUR grid. The location of profiles 1 and 2 is shown in Fig. 8a, and the profiles before and after merging the grids are shown in the panels c and d of Fig. 8. The difference of the merged SW grid with the ERS grid is within ±50 nT for both profiles, while differences exceed ±100–200 nT for the EUR grid. The variation is more prominent in profile Section 1 compared to Section 2. Anomaly differences of similar intensity (<±100 nT) also exist between the GAM, ERS and NAM grids (not shown here). Only a small difference of 8 nT exists between the SAS and AUS grids indicating consistent anomaly patterns between the grids.

5. Lithospheric field model

In many regions, lithospheric magnetic anomalies have a large spatial extent and are sufficiently strong to be mapped by low-orbiting satellites. Several models of the lithospheric magnetic field, based on satellite missions—Magsat (1979–80), Ørsted (1999), SAC-C (Nov 2000) and CHAMP (July 2000), have been produced, and they follow basically two different philosophies.

The comprehensive approach (CM4), proposed by Sabaka et al. (2004), uses POGO, Magsat, Ørsted, CHAMP and SAC-C measurements to derive a model that accounts for magnetic sources from the core to the magnetosphere and their temporal variations. However, lithospheric field representation is hampered by the consideration of noisy day-side data and is not calculated beyond 65°, giving a 600 km maximum resolution at the Earth's surface. Following the same line, various magnetic field sources are represented by the POMME model (Maus et al., 2006a) and its recent version POMME 3.1 (Maus et al., 2006 at http://www.gfz-potsdam.de/pb2/pb23/index.html) using quiet-time and night-side data only. For lithospheric field detection, considering undisturbed data from the night region greatly reduces ionospheric effects and stabilizes the model at the ground to 60°. In an attempt to reduce error and noise level in satellite data, Olsen et al. (2006) suggested resolving attitude parameters with a joint inversion and they proposed the CHAOS model. These refinements improve the representation of the secular variation (Olsen et al., 2006) but lithospheric field resolution does not exceed 50°. Despite the different approaches employed the lithospheric models are rather robust for the low harmonic degrees, but what we need here is a resolution improvement for the high degrees.

In contrast to the comprehensive approach, the second philosophy strictly focuses on the lithospheric field representation. Prior to the modelling, careful data selection and processing is performed to clean the data from non-lithospheric sources. This approach requires many independent corrections. Maus et al. (2006b) used four years of CHAMP data to produce MF4, which is derived up to 90°. Despite this resolution improvement, MF4 shows inconsistencies in the Polar Regions where data noise levels are highest. Using localized basis functions, Lesur and Maus (2006) produced the MF4x model (http://www.gfz-potsdam.de/pb2/pb23/index_e.html) which has a 60° resolution at high latitudes and a 90° resolution at mid latitudes. Recently, the fifth generation of CHAMP models, MF5, was released (Maus et al., 2007). MF5 extends to

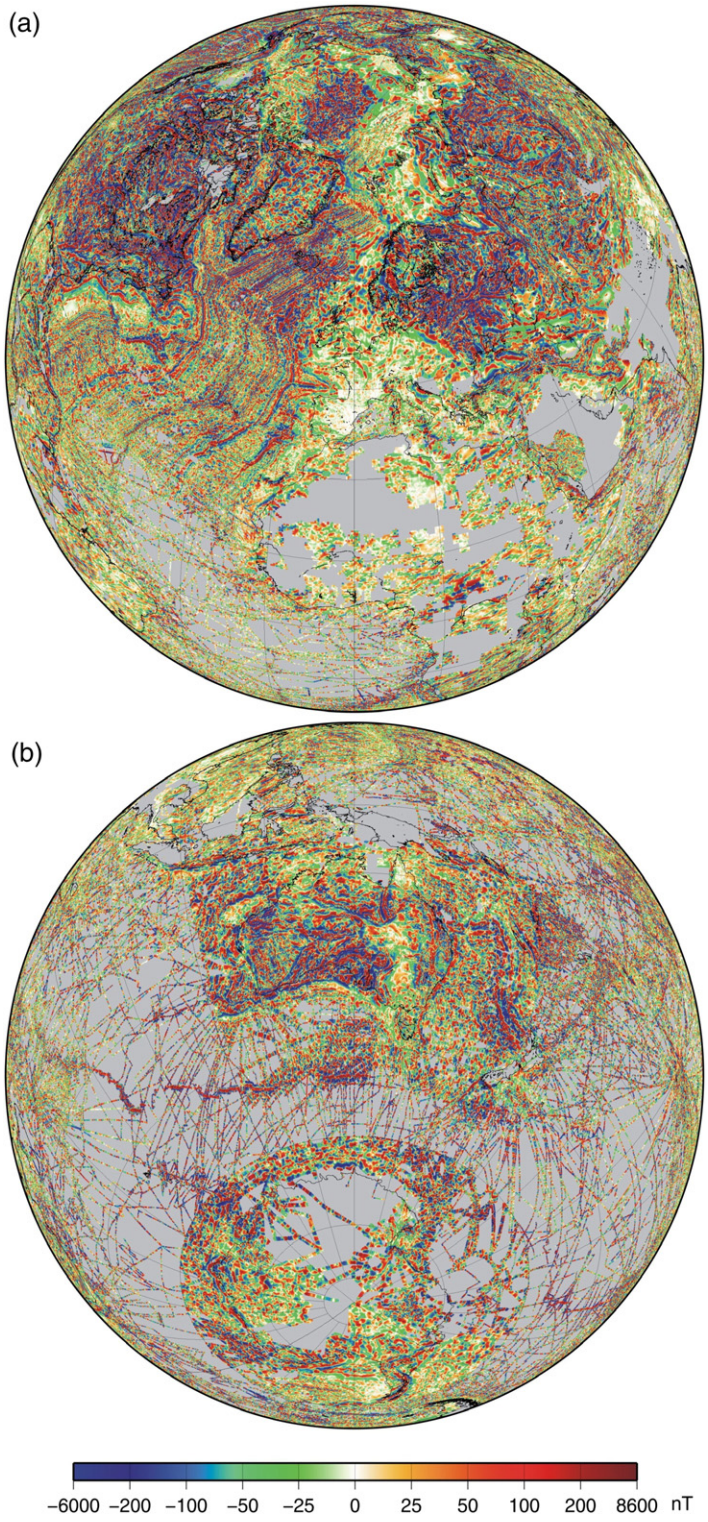

Fig. 7. Merged short wavelength (wavelength < 400 km) anomaly map of the world. Two azimuthal views one over (a) the northern and the other over (b) the southern hemisphere, is shown.

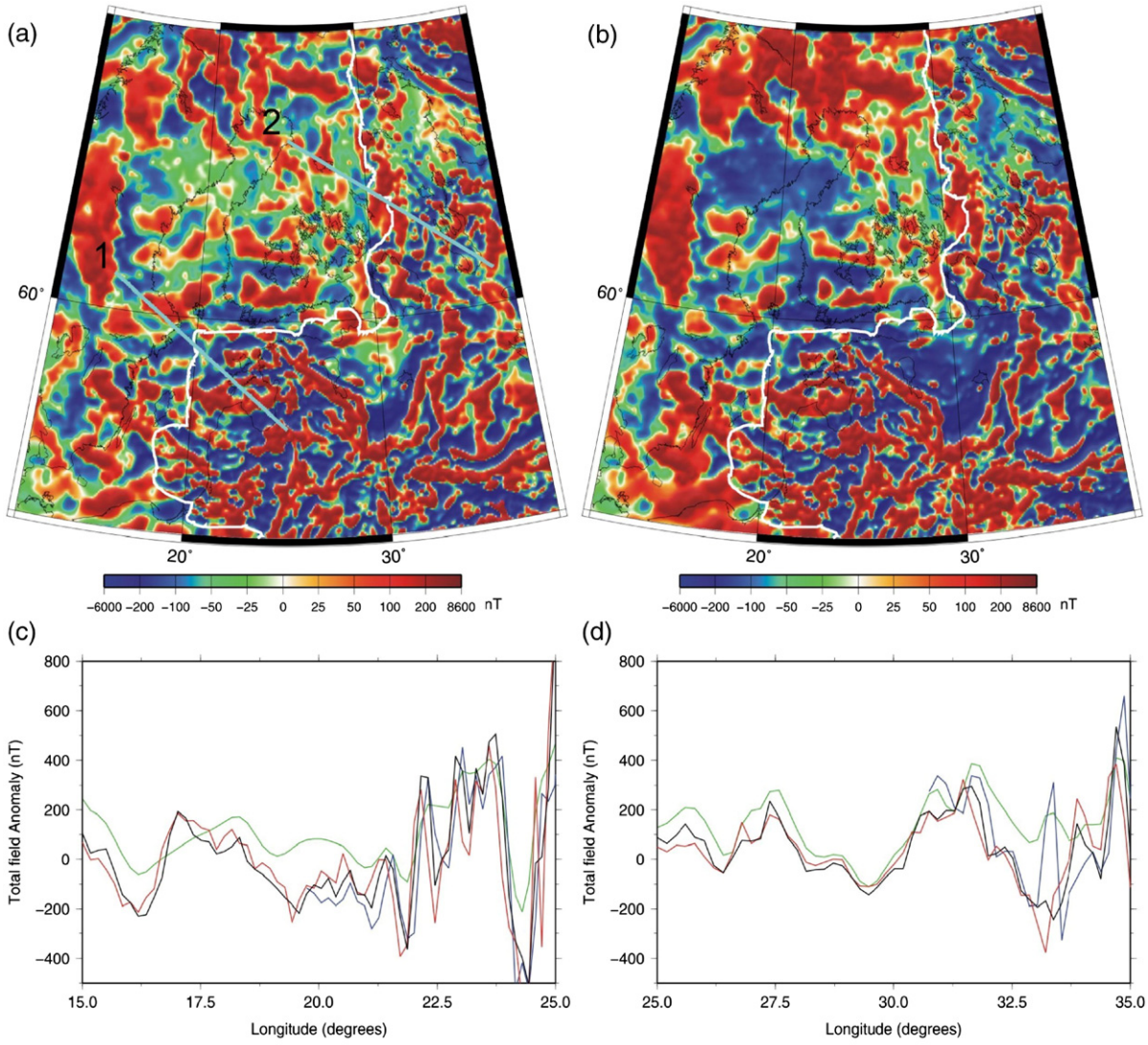

Fig. 8. A zoomed-in view of (a) the merged SW (Fig. 7) and (b) the final merged magnetic anomaly map WMAM plotted over Europe. The white line in figures shows the boundary of ERS grid and the EUR grid. Profile sections 1 and 2 are plotted in (c) and (d) respectively. The 'green' line shows the raw anomaly data for EUR while 'blue' line show the same data for ERS grid. SW merged magnetic anomaly grid is shown in 'red' line while 'black' line marks the profile for the combined SW and LW WMAM grid.

100° (400 km resolution). MF5 shows a significant improvement, especially between 60–80° latitude, compared to previous models. Also the WDMAM committee, after comparing the MF series of models, recommended using the MF5 model for the preparation of candidate models. For the substitution of large wavelengths we use MF5 to 100° (400 km resolution), which is a good choice among the available models for resolution at the ground and smoothness of the lithospheric field at 5 km altitude on the WGS84 ellipsoid. This long wavelength grid is shown in Fig. 9. An unpublished study of the Australian aeromagnetic data and various recent satellite based magnetic field models shows that MF5 reproduces anomaly features similar to the >400 km wavelength Australian magnetic anomaly data set (Gaya-Pique, Milligan, Sabaka, and Ravat, personal communication, 2006).

5.1. Substituting long wavelengths

As the long wavelength components of the global map show significant mismatch after merging (Fig. 5;

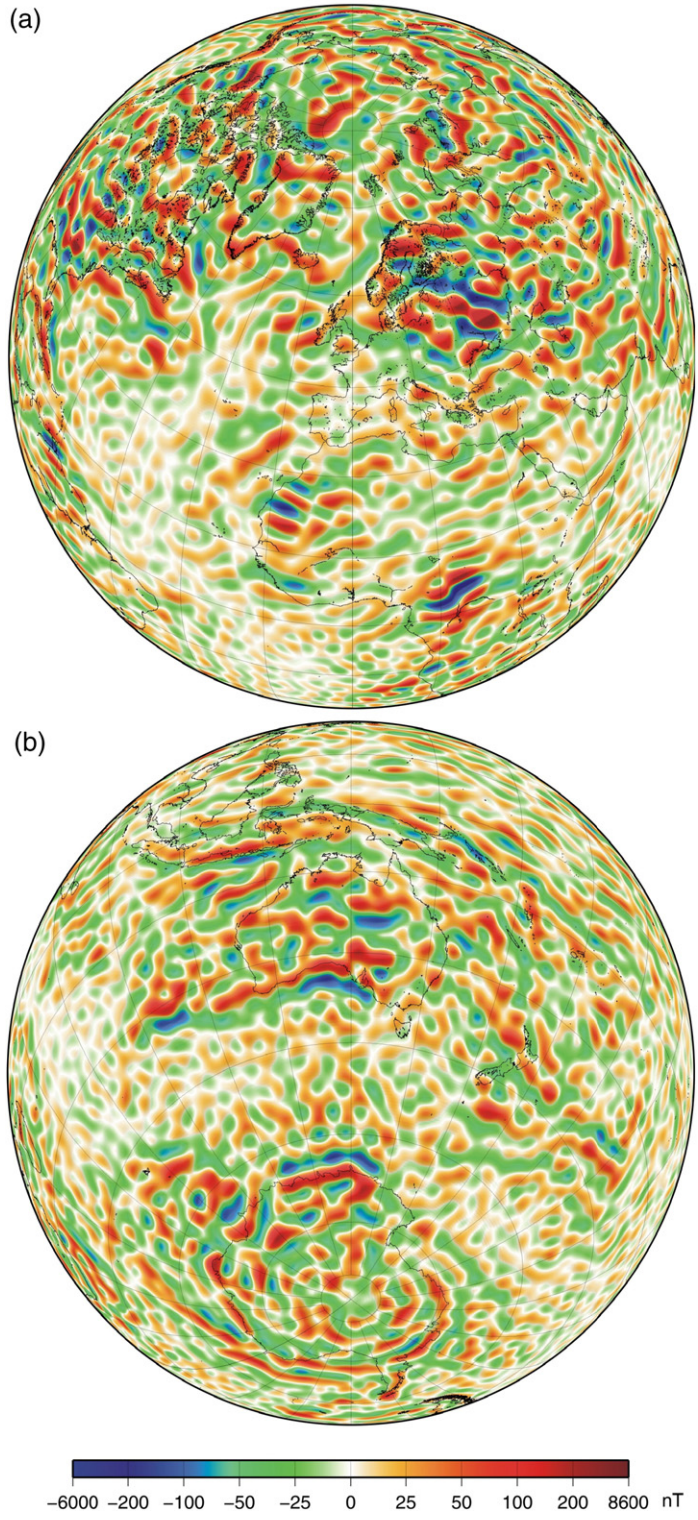

Fig. 9. MF5 model derived using CHAMP satellite data, downward continued to 5 km altitude (SH degree 16–100; wavelength >400 km). Two azimuthal views one over (a) the northern and the other over (b) the southern hemisphere, is shown.

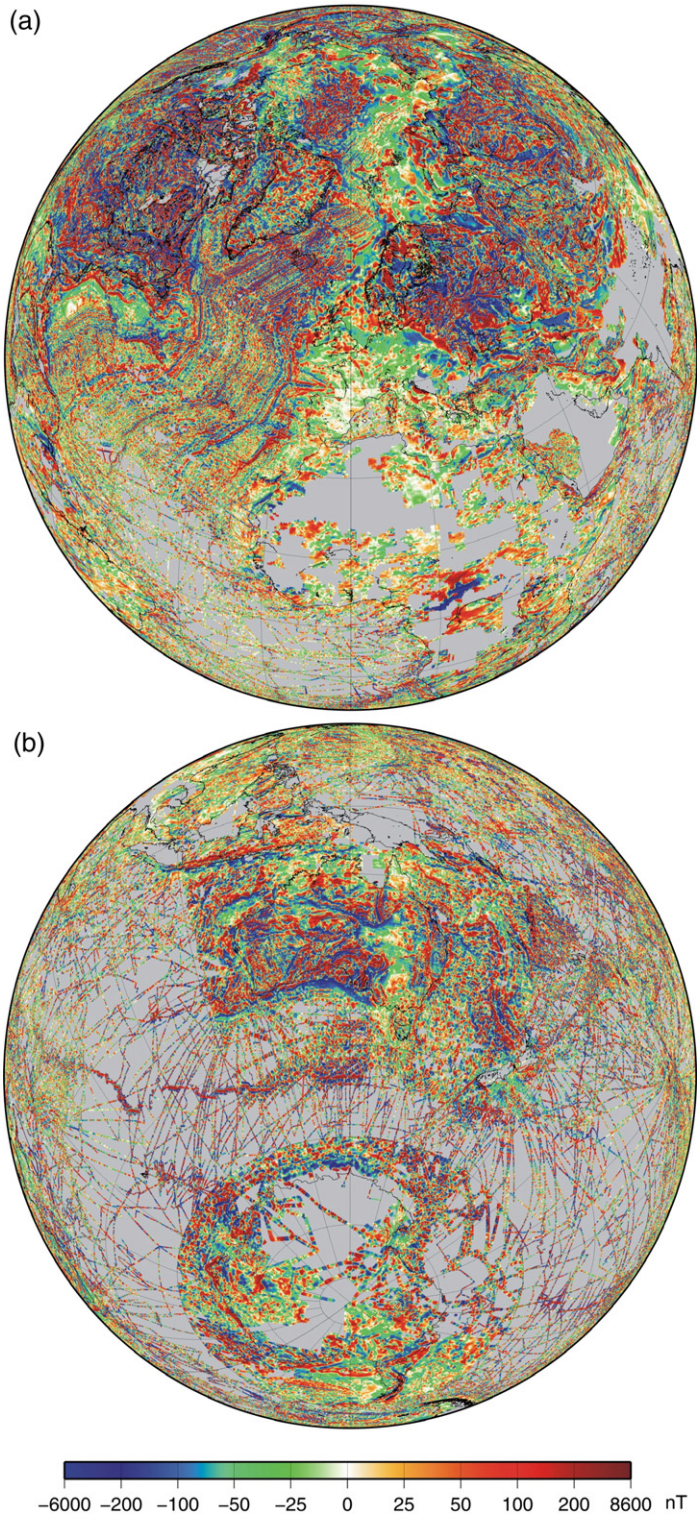

Fig. 10. World magnetic anomaly map (WMAM) produced by combining Figs. 7 and 9. Two azimuthal views one over (a) the northern and the other over (b) the southern hemisphere is shown.

Table 2), the long wavelengths are replaced by the downward-continued total field anomaly of the MF5 model (Fig. 9). The total field anomalies of the short wavelength merged magnetic anomaly map (Fig. 7) and the long wavelength component of MF5 are added to produce one of the candidate models of the world magnetic anomaly map (WDMAM). The maximum wavelength represented by the WMAM corresponds to spherical harmonic 16° or a wavelength of about 2500 km and, a minimum wavelength of 11 km at the equator, where data are available. The candidate model LEEDS-WDMAM is shown in Fig. 10. Recently, two other candidate models (Hamoudi et al., in press; Maus et al., in press) have also been published and are available from (http://www.earthref.org).

6. Conclusion

We have presented a simple approach that has been used here to compile a world magnetic anomaly map. The map is derived by combining ground-based, airborne, marine and satellite magnetic data. A prior thorough analysis of the grids was necessary to detect outliers, incorrect coordinate systems and shifts in the data, in order to merge them without generating artifacts. The simple approach we adopt here removes the long wavelengths from near-surface compilations by filtering because careful examination of the data suggest that near-surface compilations contain long wavelengths (>400 km) that differ significantly, both in strength and shape, with the adjoining compilation or global satellite derived lithospheric magnetic field models. The difference maps indicate that discrepancies are of the order of the strength of long wavelength anomalies of the merging grids. In contrast, wavelengths smaller than 400 km are naturally attenuated in the present satellite data. The MF5 magnetic field model derived from CHAMP satellite is therefore used here only to replace long wavelengths in the near-surface compilations. The prior removal of long wavelengths significantly improves the remaining short wavelength signal and facilitates merging. The analysis of sample profiles showed that small overlapping areas of the merging grids further limit the propagation of errors introduced in merging. Considering the extreme heterogeneity of some adjacent grids, differences, of the order of up to ± 100 nT are acceptable when compared to typical anomaly intensities in the range of hundreds of nT intensity.

One of the major problems encountered in the processing is the resolution heterogeneity within the individual grids themselves. This greatly hampers spectral analysis and visual inspections as tools in assessing the effective merging the grids. Thus, in the future, it would be important for regional magnetic anomaly compilers, whose products we largely rely on, to keep improving their grids.

The WDMAM project will also benefit from improved global magnetic field models. The forthcoming *Swarm* mission, selected by the European Space Agency (2004), will provide new highly accurate satellite measurements at low altitudes, and as a result we expect a great improvement in the representation of the intermediate wavelength lithospheric field. In summary, with the method proposed here, it will be possible to regularly update candidates for the WDMAM without excessive effort, in order to continuously improve the representation of the world magnetic anomalies.

Acknowledgments

We thank two anonymous referees for numerous helpful suggestions to improve this manuscript. We would like to acknowledge all geological surveys and group members listed in Table 1 who provided aeromagnetic and marine magnetic anomaly data for World Digital Magnetic Anomaly project. We kindly thank Juha Korhonen and other members of the WDMAM task force for their successful negotiations with various organisations and data holders. The CHAMP satellite mission is operated and supported by GeoForschungsZentrum Potsdam, the German Aerospace Center (DLR) and the German Federal Ministry of Education and Research (BMBF).

References

Bankey, V.A., Cuevas, D., Daniels, A.A., Finn, I., 2002. Hermandez and Project Members, Digital Data Grids for the Magnetic Anomaly Map of North America, USGS (2002), Open-File Report 02-414.

Blakely, R.J., Simpson, R.W., 1986. Approximating edges of source bodies from magnetic or gravity anomalies. Geophysics 51, 1494–1498.

Blakely, R.J., Wells, R.E., Tolan, T.L., Beeson, M.H., Trehu, A.M., Liberty, L.M., 2000. New aeromagnetic data reveal large strike-slip (?) faults in the northern Willamette Valley, Oregon. Geol. Soc. Amer. Bull. 112, 1225–1233.

Behrendt, J.C., Finn, C.A., Blankenship, D., Bell, R.E., 1998. Aeromagnetic evidence for a volcanic caldera(?) complex beneath the divide of the West Antarctic Ice Sheet. Geophys. Res. Lett. 25, 4385–4388.

ESA, 2004. Swarm — the Earth's magnetic field and environment explorers, Tech-Report. SP-1279(0).

Franke, R., 1982. Smooth interpolation of scattered data by local thin plate splines. Comp. and Maths with Appls., vol. 8, No. 4. Pergamon Press Ltd., pp. 273–281.

Golynsky, A., et al., 2002. ADMAP: a magnetic anomaly map of the Antarctica south of 60°. http://www.geology.ohio-state.edu/geophys/admap/databases.html2002.

Griscom, A., Jachens, R.C., 1989. Tectonic history of the north portion of the San Andreas fault system, California, inferred from gravity and magnetic anomalies. J. Geophys. Res. 93, 3089–3099.

Hamoudi, M., Thébault, E., Lesur, V., Mandea, M., in press. GeoForschungsZentrum Anomaly Magnetic MAp (GAMMA): A candidate model for the World Digital Magnetic Anomaly Map. Geochem. Geophys. Geosyst. doi:10.1029/2007GC001638.

Ishihara, T., Kisimoto, K., 1996. Magnetic anomaly map of East Asia 1:4,000,000., Geological Survey of Japan.

Kim, H.R.R., Von Frese, Golynsky, A., Taylor, P., Kim, J.K., 2004. Application of satellite magnetic observations for estimating near-surface magnetic anomalies. Earth Planets Space 56, 955–966.

Le Mouel, J.L., 1969. Sur la distribution des elements magne´tiques en France, PhD thesis. Univ. de Paris, Paris.

Lesur, V., Maus, S., 2006. A global lithospheric magnetic field model with reduced noise level in Polar Regions. Geophys. Res. Lett. 33, L13304.

Maus, S., Rother, M., Stolle, C., Mai, W., Choi, S., Lühr, H., Cooke, D., Roth, C., 2006a. Third generation of the Potsdam Magnetic Model of the Earth (POMME). Geochem. Geophys. Geosyst. 7, Q07008. doi:10.1029/2006GC001269.

Maus, S., Rother, M., Hemant, K., Stolle, C., Luehr, H., Kuvshinov, A., Olsen, N., 2006b. Earth's lithosphere magnetic field determined to spherical harmonic degree 90 from CHAMP satellite measurements. Geophys. J. Int. 165 (2), 319–330.

Maus, S., Luehr, H., Martin, R., Hemant, K., Balasis, G., Ritter, P., Claudia, S., 2007. Fifth-generation lithospheric magnetic field model from CHAMP satellite measurements. Geochem. Geophys Geosyst. 8, Q05013. doi:10.1029/2006GC001521.

Maus, S., Sazonova, T., Hemant, K., Fairhead, J.D., Ravat, D., in press. National Geophysical Data Center candidate for the World Digital Magnetic Anomaly Map. Geochem. Geophys. Geosyst. doi:10.1029/2007GC001643.

Olsen, N., Lühr, H., Sabaka, T.J., Mandea, M., Rother, M., Tøffner-Clausen, L., Choi, S., 2006. CHAOS — a model of the Earth's magnetic field derived from CHAMP, Ørsted, and SAC-C magnetic satellite data. Geophys. J. Int. 166 (1), 67–75.

Petkovic, P., Milligan, P., 2002. Magnetic anomaly grid of the Australian region, 3.1, Digital Canberra: Geoscience Australia. http://www.osdm.gov.au/2002.

Pilkington, M., Todoeschuck, J.P., 1993. Fractal magnetization of continental crust. Geophys. Res. Lett. 20 (8), 639–641.

Ravat, D., Whaler, K.A., Pilkington, M., Sabaka, T., Purucker, M.E., 2002. Compatibility of the high-altitude aeromagnetic and satellite-altitude magnetic anomalies over Canada. Geophysics 67, 546–554.

Ravat, D., Hildenbrand, T., Roest, W., 2003. New way of processing near-surface magnetic data: the utility of the comprehensive model of the magnetic field. Lead. Edge 22, 784–785.

Reeves, C., 2003. ITC, AAIME (Aeromagnetics of Arabia, India and the Middle East). CD ROM version.

Reeves, C.V., de Wit, M., 2000. Making ends meet in Gondwana: retracing the transforms of the Indian Ocean and reconnecting continental shear zones. Terra Nova 12, 272–280.

Sabaka, T.J., Olsen, N., Purucker, M.E., 2004. Extending the comprehensive models of the Earth's magnetic field with Oersted and CHAMP data. Geophys. J. Int. 159, 521–547.

Smith, R., Ravat, D., 2005. A CD containing selected Project MAGNET data from the time periods of 1976–1977 and 1981–1994 processed with comprehensive magnetic field model CM4, World Digital Magnetic Anomaly Map project of IAGA, Southern Illinois University Carbondale (2006), 1 CD.

Smith Jr., R., Ravat, D., 2006. Reprocessing of NGDC-Held Marine Data with the Comprehensive Magnetic Field Model (CM4). Southern Illinois University Carbondale. 2 DVDs.

Snyder, J.P., 1987. Map projections — a working manual, US Geological Survey. Professional Paper, vol. 1395.

Verhoef, J.R., Macnab, R., Roest, W., Arkani-Hamed, J., 1996. Geological Survey of Canada, Magnetic anomalies of the Arctic and North Atlantic Oceans and Adjacent Land Areas. Open file 3125a.

Vine, F.J., 1966. Spreading of the ocean floor: new evidence. Science l54, 1405–1415.

Wessel, P., Smith, W.H.F., 2004. The Generic Mapping Tools Technical Reference and Cookbook, Version 4.0, p. 132.

Whaler, K.A., 1994. Downward continuation of Magsat lithospheric anomalies to the Earth's surface. Geophys. J. Int. 116, 267–278.

Wonik, T., Trippler, K., Geipel, H., Greinwald, S., Pashkevitch, I., 2001. Magnetic anomaly map for Northern, Western and Eastern Europe, Terra Nova, vol. 13, pp. 203–213.

Zietz, I., 1982. Composite magnetic anomaly map of the United States; Part A, Conterminous United States: US Geological Survey investigation Maps GP-954-A, 2 sheets, scale 1:2,500,000, 59 pp.